The Astrophysical Journal, 861:41 (6pp), 2018 July 1 https://doi.org/10.3847/1538-4357/aac6da

Polarization of Trappist-1 by the Transit of Its Planets

Sujan Sengupta
Indian Institute of Astrophysics, Koramangala 2nd Block, Bangalore 560 034, India; sujan@iiap.res.in
Received 2018 February 10; revised 2018 April 9; accepted 2018 May 16; published 2018 June 29

Abstract

Being the first, and currently the only, multiple planet hosting dwarf star that is sufficiently cool to form condensate clouds in its atmosphere, Trappist-1 provides a unique opportunity to test the efficiency of image polarimetry as a tool to detect and characterize exoplanets around L- and late M-dwarfs and exomoons around directly imaged self-luminous giant exoplanets. Although scattering of light by atmospheric dust particles should produce a significant amount of linear polarization in the far optical and near infrared, the disk-averaged net detectable polarization of the star must be zero owing to spherical symmetry. However, the transit of its planets would give rise to significant asymmetry and produce phase-dependent polarization with the peak polarization occurring at the inner contact points of planetary transit ingress and egress epochs. Adopting the known stellar and planetary physical parameters and employing a self-consistent cloudy atmosphere model of the M8 dwarf star, the transit polarization profiles and the expected amount of polarization of Trappist-1 during the transit phase of each individual planet, as well as that during the simultaneous transit of two planets, are presented in this paper. It is emphasized that the amount of polarization expected is within the detection limit of a few existing facilities. If polarization is detected confirming the prediction, time-resolved image polarimetry will emerge as a potential tool to detect and characterize small planets around cloudy ultra-cool dwarfs.

Key words: polarization – stars: individual (TRAPPIST-1) – stars: low-mass

1. Introduction

Two decades after the first confirmed discovery of planets outside the solar system (Wolszczan & Frail 1992; Wolszczan 1994; Mayor & Queloz 1995), more than 3000 planets of different size, mass, and composition have been detected. Most of these planets are found to be orbiting around solar-type stars. It is known that red dwarfs and brown dwarfs account for about 80% of the stellar population in our galaxy (Apai 2013). As a consequence, searches for planets around these ultra-cool dwarfs will enable tests of the formation models because they will provide a complete and comprehensive understanding of the planetary architecture as a function of the mass of the host. Therefore, the discovery of seven Earth-sized planets transiting the M8V star Trappist-1 (Gillon et al. 2016, 2017) is a significant step. Trappist-1 (2MASS J23062928-0502285) is located 12.14 pc from the Sun (Van Grootel et al. 2018). It is the first planetary system found to transit a very low mass, Jupiter-sized star. The favorable planet-to-star ratio offers the opportunity to probe their atmospheric properties with both current and next-generation telescopes (Barstow & Irwin 2016; de Wit et al. 2016). Furthermore, a unique system such as Trappist-1 enables us to test planet formation and evolution theories and to investigate the prospects for habitability among Earth-sized exoplanets orbiting cool M-dwarfs.

The atmospheres of dwarf stars with spectral type M7 and later are cold enough for the condensation of the silicate cloud (Tsuji et al. 1996; Ackerman & Marley 2001; Allard et al. 2001). The spectra of L-dwarfs are well explained by the inclusion of condensate clouds of various species such as iron, forsterite, and enstatite (Cushing et al. 2008; Marley & Robinson 2015). Scattering of thermal radiation by these dust particles in the visible atmosphere of ultra-cool dwarfs gives rise to a significant amount of linear polarization in the far optical and infrared regions. Linear polarization has been detected in the optical bands from a significant number of L-dwarfs covering almost the entire range of spectral types L0–L8 (Ménard et al. 2002; Zapatero Osorio et al. 2005; Tata et al. 2009; Zapatero Osorio et al. 2011; Miles-Páez et al. 2013). Scattering by horizontally homogeneous clouds in the atmosphere of a rotation-induced oblate L-dwarf can explain the observed polarization (Sengupta & Krishan 2001; Sengupta 2003; Sengupta & Kwok 2005; Sengupta & Marley 2010).

Similar to the L-dwarfs, Trappist-1, a dwarf star of M8V spectral type with an effective temperature of about 2500 K and about the size of a brown dwarf, is expected to have a thin cloud in the upper atmosphere. Therefore, the thermal radiation of Trappist-1 should also be linearly polarized due to scattering by dust particles. However, being a slow rotator with a spin rotation period as high as 79.2 hr (Luger et al. 2017), the object should be almost spherical and hence the disk-integrated polarization of Trappist-1 should be negligible. However, transit by the planets would give rise to significant asymmetry by partially blocking the stellar disk during the transit epoch (Sengupta 2016). As a consequence, transit of planets around Trappist-1 would give rise to net nonzero time-dependent disk-integrated polarization. Since Trappist-1 is presently the only discovered ultra-cool dwarf with a cloudy atmosphere and has a system of seven rocky planets, it can serve very well as a test object for verifying the potential of image polarimetry as a tool to detect planets around similar late M-dwarfs and L-dwarfs as well as exomoons around self-luminous giant exoplanets.

In this paper, the transit polarization profiles for Trappist-1 with specific predictions of the expected amount of polarization are presented. In Section 2, the employed atmosphere model and the adopted formalism for calculating the transit polarization are described. In Section 3, the results are discussed and, in Section 4, it is concluded that, if confirmed, time-resolved image polarimetry will open up a new avenue to detect and characterize exoplanets around ultra-cool dwarfs.

2. Method for Calculating the Transit Polarization

The disk-integrated polarization of a spherical star is zero. However, when a planet transits the star, the net polarization during the transit is nonzero owing to the asymmetry caused by partial blocking of the stellar disk. The transit polarization of the star is the product of the intensity and scattering polarization at each radial point along the disk of the star with the fractional circumference occulted by the projection of the planet over the surface of the star. The disk-integrated polarization during the transit phase is given by Sengupta & Marley (2016), Sengupta (2016), Wiktorowicz & Laughlin (2014), and Carciofi & Magalhaes (2005):

$$p(t,\lambda) = \frac{1}{F}\int_{r_1}^{r_2} 2\sqrt{\frac{[(1-\mu^2)^{1/2} - r_m(t)]^2 - w^2}{1-\mu^2}} \times I(\mu,\lambda)p(\mu,\lambda)\mu d\mu, \quad (1)$$

where t is the time since mid-transit and F is the flux of the unobscured star at a given wavelength or band. In the above expression, $I(\mu, \lambda)$ and $p(\mu, \lambda)$ are the wavelength dependent specific intensity and polarization, respectively, along μ, $\mu = \cos\theta = \sqrt{1-r^2}$ with θ being the angle between the normal to the surface of the star and the line of sight and r being the radial points along the disk of the primary, $0 \leqslant r \leqslant 1$, $r_1 = \sqrt{1-[r_m(t)+w]^2}$ and $r_2 = \sqrt{1-[r_m(t)-w]^2}$, $r_m(t)$ is the instantaneous position of the center of the planet and is given by

$$r_m(t) = \left[b^2 + 4\{(1-2w)^2 - b^2\}\left(\frac{t}{\tau}\right)^2\right]^{1/2}, \quad (2)$$

where $b = a\cos i/R_\star$ is the impact parameter of the planet with a circular orbit of radius a and the orbital inclination angle i and $R_\star$ is the radius of the star, $w = R_P/R_\star$ is the ratio of the planetary radius (R_P) to the radius of the star and τ is the total transit duration given by Scharf (2009)

$$\tau = \frac{P}{\pi}\sin^{-1}\left[\frac{R_p}{a}\left\{\frac{(1+w)^2 - b^2}{1-\cos^2 i}\right\}^{1/2}\right], \quad (3)$$

P being the orbital period of the planet. The physical parameters used are presented in Table 1. These are derived by using the values of R_P, a, P, and i as given in Gillon et al. (2017).

In order to calculate the specific intensity $I(\mu, \lambda)$ and scattering polarization $p(\mu, \lambda)$ for Trappist-1, I have employed the commonly used one-dimensional, non-gray, hydrostatic and radiative-convective atmospheric model for the relatively hotter L-dwarfs developed by Ackerman & Marley (2001), Marley et al. (2002), and Freedman et al. (2008). This model fits reasonably well the spectra and photometry of a large number of cloudy L-dwarfs at a wide range of wavelengths covering near-optical to mid-infrared regions (Marley & Robinson 2015). The effective temperature of Trappist-1 is $T_{\rm eff} = 2516 \pm 41$ K and surface gravity $g = 1686.55\,{\rm ms}^{-2}$ (Van Grootel et al. 2018). I adopt a grid of the atmosphere model with $T_{\rm eff} = 2400$ K and $g = 1000\,{\rm ms}^{-2}$. The slightly lower temperature compensates the cloud thickness for a lower surface gravity and hence the model atmosphere does not differ significantly from that of the actual atmosphere of Trappist-1. In fact, it is known that the synthetic spectra of L-dwarfs or ultra-cool dwarfs such as Trappist-1 (M8) remain the same for a wide range of surface gravity. Figure 1 (upper panel) presents a comparision of the theoretical spectrum to the observed spectral energy distribution of Trappist-1 (Burgasser et al. 2015). Owing to the low spectral resolution of the thoeretical spectrum, a better fit to the observed spectrum at wavelengths longer than 1.4 μm is not achieved. However, polarization changes slowly with wavelength and this resolution is adequate for the present purpose. Note that the polarization profiles are presented in I- and J-bands by using the response functions of SDSS filters. The I- and J-bands cover a wavelength region from 0.65 to 1.4 μm. Therefore, the models serve the present purpose well.

Table 1
Physical Parameters of the Seven Planets Transiting Trappist-1

Planets	$w = R_P/R_\star$	$b = a\cos i/R_\star$	τ (minutes)
Trappist-1b	0.085	0.125	36.48
Trappist-1c	0.083	0,161	42.42
Trappist-1d	0.060	0.172	49.18
Trappist-1e	0.072	0.126	57.34
Trappist-1f	0.082	0.380	62.52
Trappist-1g	0.088	0.419	68.425
Trappist-1h	0.059	0.454	75.697

In this atmosphere model, the spatially uniform dust cloud is included self-consistently. The efficiency of sedimentation of cloud particles in the atmospheric models is controlled through a scaling factor $f_{\rm sed}$. In the present work, I adopt $f_{\rm sed} = 2.0$ (Cushing et al. 2008; Stephens et al. 2009), which incorporates a moderately thick condensate cloud. However, in order to investigate how sensitive the polarization is to the cloud opacity, I have also calculated polarization with 5%, 10%, and 15% increases in the dust opacity without changing gas opacity in the model. This does not affect the emergent spectra of the star as shown in Figure 1 (bottom panel) but alters the amount of polarization significantly.

The detailed formalisms as well as the numerical methods for calculating the angle dependent intensity and linear polarization are described in Sengupta & Marley (2009, 2010).

3. Results and Discussions

The formation of dust grains in the cloudy atmosphere of ultra-cool dwarfs provides an additional scattering opacity to the gas opacity. The thermal radiation of such cloudy dwarf stars and self-luminous giant exoplanets is polarized by dust scattering in the far optical and infrared wavelengths (Sengupta & Marley 2010; Marley & Sengupta 2011). The net nonzero disk-integrated polarization of such cloudy objects arises only during the transit epoch unless the object is nonspherical. However, slow spin rotation ensures that Trappist-1 has almost perfect spherical symmetry and hence the disk-integrated polarization should be zero during the nontransit epoch.

As depicted in Figures 2 and 3, the polarization increases significantly with the increase in dust opacity even by 5% of

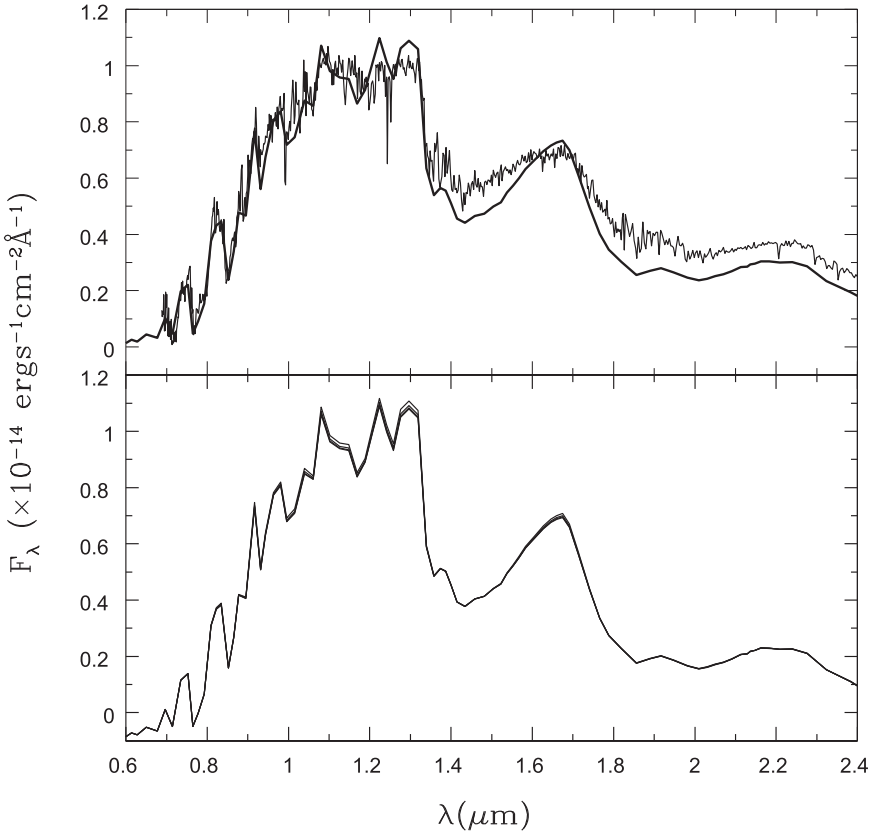

Figure 1. Top panel: comparison of the model spectrum to the observed spectrum of Trappist-1. The thick line is the theoretical model spectrum and the thin line is the observed spectral energy distribution (Burgasser et al. 2015). Bottom panel: comparison of the original model spectrum to those with 5%, 10%, and 15% increases in the dust opacity.

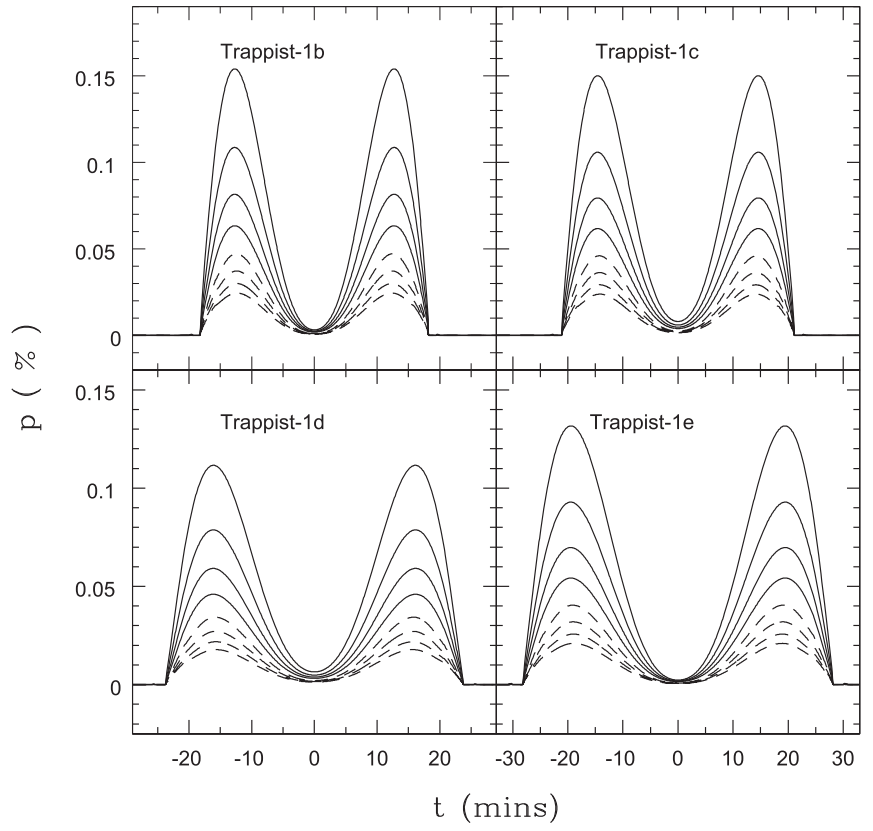

Figure 2. I- and J-band polarization of the star Trappist-1 due to the transit of its planets Trappist-1b, Trappist-1c, Trappist-1d, and Trappist-1e. The solid lines represent the polarization profile in J-band, while the broken lines represent that in I-band. From bottom to top, the solid (and broken) lines show the polarization with the (1) original atmosphere model with $f = 2$, (2) 5%, (3) 10%, and (4) 15% increased dust opacity.

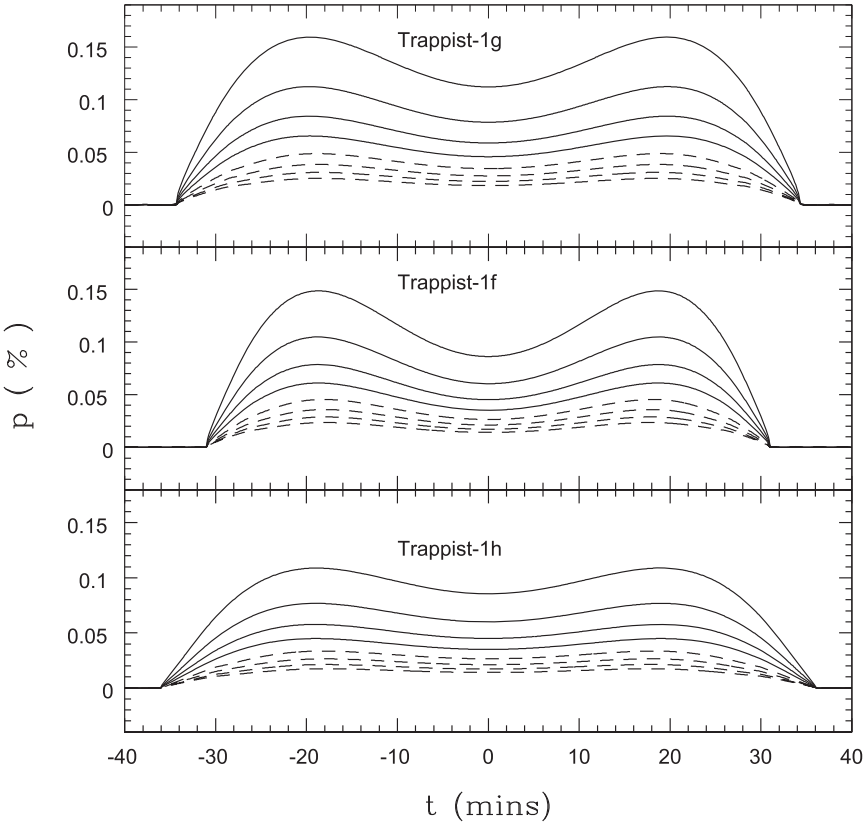

Figure 3. Same as Figure 2 but due to the transit of planets Trappist-1f, Trappist-1g, and Trappist-1h.

the original cloud model. The scattering opacity is determined by a balance between the upward turbulent diffusion and downward transport by sedimentation of condensates and gas. These are governed by the surface gravity and effective temperature and hence the polarization varies with different effective temperature and surface gravity. While polarization reduces with the decrease in surface gravity, a decrease in temperature causes the cloud base to shift downward yielding a larger column of dust grains in the observed atmosphere and hence the polarization increases with the decrease in effective temperature (Sengupta 2016). Therefore, while the adopted effective temperature of Trappist-1 is slightly less than the actual value, a reduced value of surface gravity considered should yield the expected amount of polarization of Trappist-1. However, the actual cloud opacity is highly model dependent and so the polarization profile is calculated with varying scattering opacity. The peak polarization at the inner contact points of the transit ingress/egress phase is thus determined by the scattering opacity as well as the size of the transiting planet. The amount of polarization is also wavelength dependent. Polarization is found to be maximum at J-band.

As discussed in Sengupta & Marley (2016) and Sengupta (2016), the general feature of transit polarization of any star is the double peaked polarization profile that arises because the maximum polarization occurs at the inner contact points of transit ingress/egress phases. For central transit, i.e., when the impact parameter $b = 0$, the projected position of the center of the planet coincides with the center of the star during mid-transit, giving rise to a symmetry to the projected stellar disk. Hence the disk-integrated polarization for central transit or transit with a small value of the impact parameter b is zero or negligibly small during mid-transit. Although the orbital inclination angles of all seven planets are almost the same, owing to a closer orbit, the values of the impact parameters of Trappist-1b, Trappist-1c, Trappist-1d, and Trappist-1e are quite small (see Table 1) and hence the amount of polarization during mid-transit of these four planets is negligibly small, as shown in Figure 2. However, as the orbital distance a increases, the impact parameter b increases for $i \neq 0$ making the transit significantly off center. Therefore, the polarization is nonzero during the whole transit epoch, including the mid-transit time of Trappist-1f, Trappist-1g, and Trappist-1h (see Figure 3).

The polarization increases sharply from zero at the outer contact point and peaks at the inner contact point of transit ingress. Similarly, the polarization falls rapidly to zero at the outer contact point from its peak value at the inner contact point of transit egress. Therefore, the polarization profile can provide the ingress/egress duration $\tau_{\rm ingress/egress}$. The asymmetry to the stellar disk decreases as the planet moves to the center ($t = 0$) from the limb ($t = \pm\tau/2$) of the stellar disk. Hence the disk-integrated polarization decreases. However, the peak polarization at the inner contact points of transit ingress/egress phases is independent of the impact parameter but depends on the ratio of the planetary to stellar radii.

The repeated occurrence of nonzero polarization with double peak would provide the orbital period of the planets. The total transit duration can be found from the transit polarization profile and the impact parameter b for a given radius of the star and orbital distance of the planet can be determined from the polarization during the mid-transit at $t = 0$. Hence, the duration

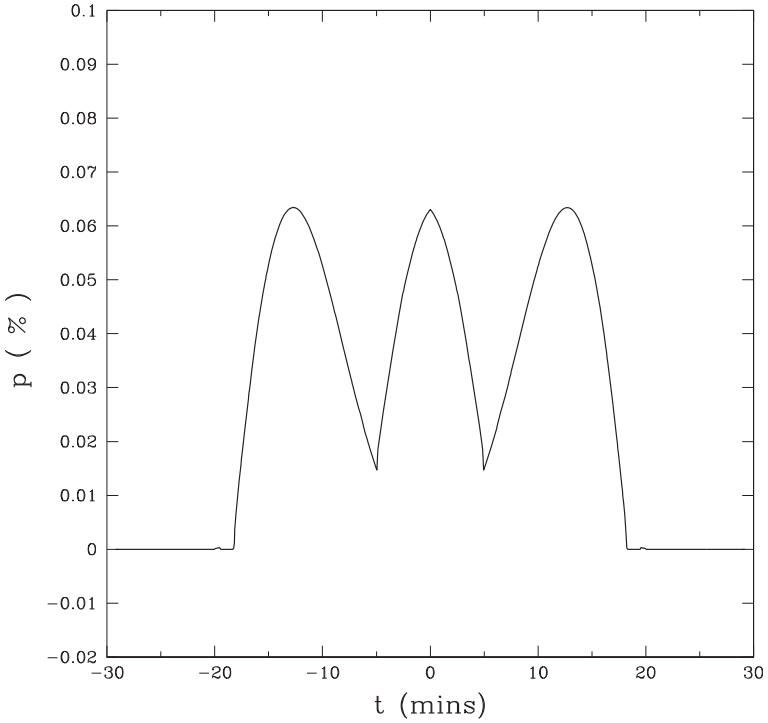

Figure 4. Polarization profile during simultaneous transits of Trappist-1b and Trappist-1c. Trappist-1b is at mid-transit epoch ($t = 0$) when Trappist-1c is at the inner contact point of the transit ingress epoch.

of the transit ingress/egress phase will provide an estimation of the size of the planet independent of any limb-darkening model by using the following expression:

$$\frac{\tau_{\rm ingress/egress}}{\tau_{\rm total}} = \frac{1}{2} - \sqrt{\frac{1}{4} - \frac{w}{(1+w)^2 - b^2}}. \quad (4)$$

Such a way of estimating the physical parameters of the transiting planet will serve as a complement to and check for the transit method. Furthermore, any stellar activity such as a flare may cause difficulties in confirming the detection of a planet through the transit method. However, such activities would not affect the polarization profile in the infrared. Hence time-resolved image polarimetry may be advantageous over the transit method in detecting planets around cloudy ultra-cool dwarfs.

Finally, Trappist-1 has a compact planetary system with several planets orbiting close to the star. Therefore, occasionally two or three planets transit the star simultaneously (Gillon et al. 2016). Simultaneous transit alters the symmetry and hence the polarization profile. In Figure 4, the polarization profile is presented for the case when the planet Trappist-1b attains its mid-transit phase while the planet Trappist-1c touches the inner contact point of its ingress phase. During the mid-transit of Trappist-1b, the symmetry would otherwise give rise to zero polarization as shown in Figure 2, but the transit of Trappist-1c would provide the necessary asymmetry and hence the polarization peaks even during the mid-transit ($t = 0$) of Trappist-1b. Therefore, a triple peak polarzation profile arises in such a scenario. Similarly, I consider another extreme case when one planet reaches the inner contact point of its egress phase, while the second one reaches the inner contact point of its ingress phase. Under such a situation, the polarization at the inner contact point of the transit egress epoch of one planet would be the sum of the peak polarization during the inner contact point of the transit ingress/egress epoch of individual planets as shown in Figure 5. Although such occasional events would favor polarimetric observation and detection, repeat image polarimetry during the transit phase of individual planet is required to estimate the physical properties of the planet.

4. Conclusions

In this article, I have presented the transit polarization profiles of Trappist-1 during the individual transit of all seven planets around it and estimated the expected peak polarization at the inner contact points of transit ingress/egress phase for each planet. Polarization profiles during simultaneous transits of two planets are also presented. For this purpose, the atmospheric model appropriate for Trappist-1 is employed. The theoretical spectrum calculated by using the model atmosphere is compared with the observed spectral energy distribution of Trappist-1 at the optical. I- and J-band linear polarization due to scattering by dust grains in the atmosphere of Trappist-1 is calculated by solving the multiple-scattering vector radiative transfer equations. The model estimation predicts a detectable amount of transit polarization in both I- and J-bands of Trappist-1 by the transit of all the planets orbiting it.

Usually it is difficult to detect exoplanets around ultra-cool dwarfs by using the techniques that are employed to look for exoplanets around solar-like stars, e.g., radial velocities, transits, direct imaging, or micro-lensing. Thus, the confirmation of the polarimetric modulation depicted in Figures 2 and 3 will open up a new and potential avenue for the search and characterization of exoplanets around ultra-cool dwarfs. Trappist-1 is currently the only target with the correct properties to investigate the prediction. The predicted amount of polarization can easily be detected by several existing

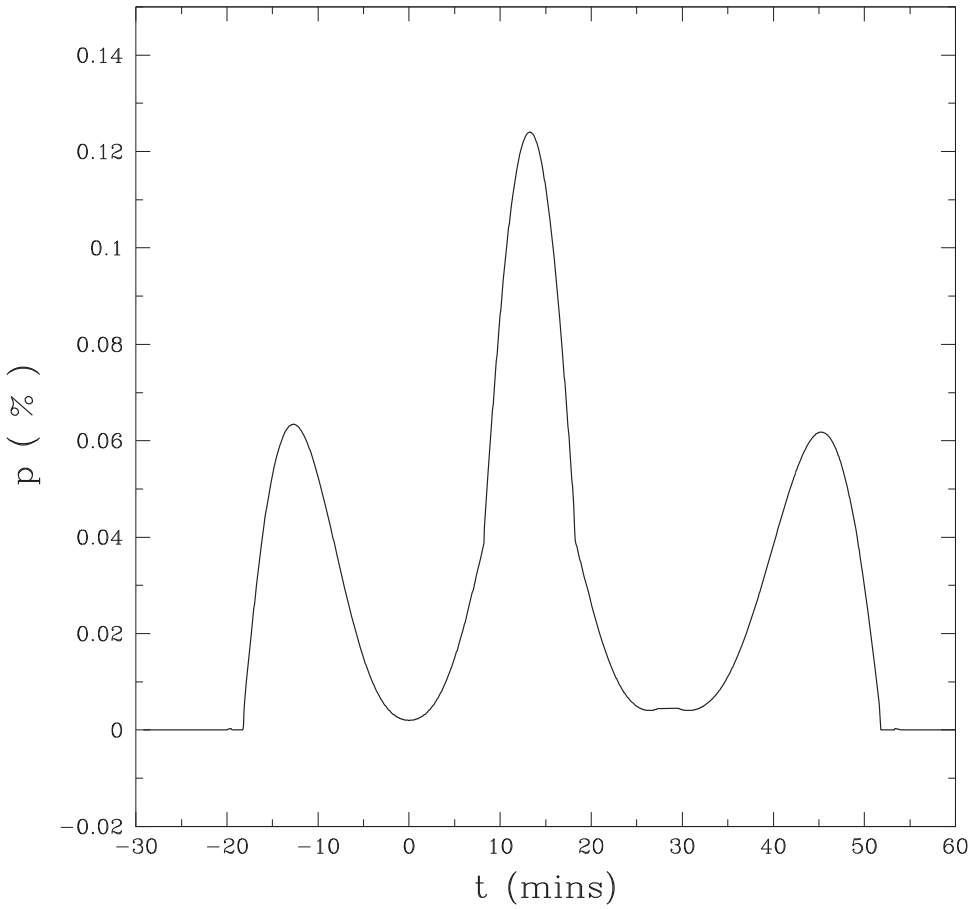

Figure 5. Polarization profile during simultaneous transits of Trappist-1b and Trappist-1c. Trappist-1b is at the inner contact point of its egress epoch, while Trappist-1c is at the inner contact point of its ingress epoch. $t = 0$ is the mid-transit epoch of Trappist-1b.

facilities, including FORS2 on board VLT and LIRIS on board WHT.

I thank Mark S. Marley for kindly providing the atmosphere model data and Adam Burgasser for kindly providing the observed spectrum of Trappist-1. Thanks are due to Enric Palle for many useful discussions and to the reviewer for providing critical comments and valuable suggestions.

ORCID iDs

Sujan Sengupta https://orcid.org/0000-0002-6176-3816

References

Ackerman, A., & Marley, M. S. 2001, ApJ, 556, 872
Allard, F., Hauschildt, P. H., Alexander, D. R., et al. 2001, ApJ, 556, 357
Apai, D. 2013, AN, 334, 57
Barstow, J. K., & Irwin, P. G. J. 2016, MNRAS, 461, L92
Burgasser, A. J., Logsdon, S. E., Gagn, J., et al. 2015, ApJS, 220, 18
Carciofi, A. C., & Magalhaes, A. M. 2005, ApJ, 635, 570
Cushing, M. C., Marley, M. S., Saumon, D., et al. 2008, ApJ, 678, 1372
de Wit, J., Wakeford, H. R., Gillon, M., et al. 2016, Natur, 537, 69
Freedman, R. S., Marley, M. S., & Lodders, K. 2008, ApJS, 174, 71
Gillon, M., Jehin, E., Lederer, S. M., et al. 2016, Natur, 533, 221
Gillon, M., Triaud, A. H. M. J., Demory, B., et al. 2017, Natur, 542, 456
Luger, R., Sestovic, M., Kruse, E., et al. 2017, NatAs, 1, 129
Marley, M. S., & Robinson, T. D. 2015, ARA&A, 53, 279
Marley, M. S., & Sengupta, S. 2011, MNRAS, 417, 2874
Marley, M. S., Seager, S., Saumon, D., et al. 2002, ApJ, 568, 335
Mayor, M., & Queloz, D. 1995, Natur, 378, 355
Ménard, F., Delfosse, X., & Monin, J.-L. 2002, A&A, 396, L35
Miles-Páez, P. A., Zapatero Osorio, M. R., Pall, E., & Peña Ramirez, K. 2013, A&A, 556, 125
Scharf, C. A. 2009, Extrasolar Planets and Astrobilogy (Sausalito, California: Univ. Science Books) Ch. 9
Sengupta, S. 2003, ApJL, 585, L155
Sengupta, S. 2016, AJ, 152, 98
Sengupta, S., & Krishan, V. 2001, ApJL, 561, L123
Sengupta, S., & Kwok, S. 2005, ApJ, 625, 996
Sengupta, S., & Marley, M. S. 2009, ApJ, 707, 716
Sengupta, S., & Marley, M. S. 2010, ApJL, 722, L142
Sengupta, S., & Marley, M. S. 2016, ApJ, 824, 76
Stephens, D. C., Leggett, S. K., Cushing, M. C., et al. 2009, ApJ, 702, 154
Tata, R., Martín, E. L., Sengupta, S., et al. 2009, A&A, 508, 1423
Tsuji, T., Ohnaka, K., & Aoki, W. 1996, A&A, 305, 1
Van Grootel, V., Fernandes, C. S., Gillon, M., et al. 2018, ApJ, 853, 30
Wiktorowicz, S. J., & Laughlin, G. P. 2014, ApJ, 795, 12
Wolszczan, A. 1994, Sci, 264, 538
Wolszczan, A., & Frail, D. A. 1992, Natur, 355, 145
Zapatero Osorio, M. R., Béjar, V. J. S., Goldman, B., et al. 2011, ApJ, 740, 4
Zapatero Osorio, M. R., Caballero, J. A., & Béjar, V. J. S. 2005, ApJ, 621, 445